Rev. Adv. Mater. Sci. 29 (2011) 31-53

# MEASURING AND ANALYZING LEAKAGE CURRENT FOR OUTDOOR INSULATORS AND SPECIMENS

**Dionisios Pylarinos[1], Kiriakos Siderakis[2] and Eleftheria Pyrgioti[1]**

[1]High Voltage Laboratory, Department of Electrical & Computer Engineering, University of Patras, University Campus, 26500, Rio, Patras, Greece
[2]Technological Educational Institute of Crete, Department of Electrical Engineering, 710 04, Iraklion Crete, Greece

*Received: April 06, 2011*

**Abstract.** Outdoor insulation represents an important component of electric power transmission and distribution systems considering that a single insulator failure can result to an excessive outage of the power system. Different insulator designs and materials are employed by power corporations and their behavior is investigated and tested in lab and field tests as well as during service conditions. Specimens (rods and plates) are also tested when researchers focus on investigating certain phenomena of surface activity or materials' performance without being influenced by the insulator design. The performance of insulators is strongly linked with local conditions especially related to the accumulation of pollutants and the wetting mechanisms present. Leakage current is a well established tool to monitor and investigate surface electrical activity, which is strongly correlated to surface and material condition, experienced pollution and local conditions, and, thus, the overall performance of insulators. The scope of this paper is to review leakage current monitoring conducted by different researchers worldwide in respect to the variety of applications, the waveform shapes recorded, the correlation of waveform shapes and surface activity, the techniques applied on leakage current waveforms, the extracted and measured values, the derived conclusions and overall significance of leakage current as a monitoring and investigating tool.

## 1. INTRODUCTION

Outdoor insulation represents a rather important component of electric power transmission and distribution systems, considering that a single insulator failure can result to an excessive outage of the power system. Various types of stresses (electrical, mechanical, environmental etc.) apply to outdoor insulators during service. Among them a phenomenon known as insulators' pollution is probably one of the most influential mechanisms experienced. The term pollution refers to the deposition, on the insulator's surface, of contaminants capable of developing a surface electrical conductivity, which further determines the voltage distribution along the insulator. This is a major change in the behavior of an insulator and the developed surface activity may, under favorable conditions, even lead to a flashover.

Pollution is correlated with various local conditions, considering the possible transfer mechanisms, e.g. neighboring facilities (plants), weather (wind, humidity, rain), general location (islands and coastal areas, desert areas, areas of high amplitude etc). In terms of conductivity two different types of have been identified [1]. The first, type A, describes solid pollution with a non-soluble component. In this case the development of surface conductivity requires the participation of a wetting agent. This type is usually associated with inland, desert or industrially polluted areas but it can also arise in coastal areas where a dry layer builds up and then rapidly becomes wetted by drizzle, fog, mist or dew. The second, type B, refers to the deposition of liquid electrolytes on the insulator, with little or no non-soluble components, which are already conductive

Corresponding author: Dionisios Pylarinos, e-mail: dpylarinos@yahoo.com

upon deposition. It is usually associated with coastal areas but can also arise in case of crop spraying, chemical mists and acid rain. Combinations of the two types can also arise.

In case of both pollution types, pollutants are either conductive (type B) or become conductive when wetted (type A) and therefore the result in both cases is the flow of leakage current (LC) through the conductive pollution film present on the insulator's surface [1-3]. The flow of this leakage current heats up the surface and as a result parts of the pollution layer begin to dry out. Drying is not uniform and areas of higher resistance, called dry bands, are formatted and interrupt the flow of leakage current. The applied voltage along the insulator is redistributed and it is mainly applied across the dry bands, resulting to the breakdown of the air surrounding. At this stage, arcs that occur bridge the dry bands and, thus, part of the leakage distance. Consequently, the surface conductivity is formed by arcs which are electrically in series with the resistance of the pollution layer that is not bridged. If the resistance of the undried part of the pollution layer is low enough, arcs may burn continuously and extend along the insulator. This decreases the resistance in series with the arcs, increases the current and permits the bridging of more of the insulator's surface. Ultimately, under favorable conditions, the phenomenon may lead to flashover.

In order to suppress the phenomenon development, many methods have been employed [3]. Among them the use of composite materials, instead of the traditionally employed porcelain and glass, is a quite promising solution. The improvement lies to the experienced surface behavior, which is water repellant and thus prevents the formation of a conductive film on the insulator's surface, by retaining water in the form of scattered droplets. However, such materials exhibit cycles of hydrophobicity loss and recovery [4]. During hydrophobicity loss periods, the insulator behaves as hydrophilic and surface activity follows the same basic steps towards flashover, which may occur if favorable conditions exists and hydrophobicity is not recovered in time.

A special case is ice accretion on insulators [3]. Surface activity towards flashover is illustrated in leakage current in this case also. Flashover occurs usually when a water film is present on the surface of the ice. One frequent situation is when ice has accreted at low temperature (e.g. during the night) and then its surface starts to melt when the ambient temperature rises above freezing. Pre-contamination, superimposed pollution and freezing-water conductivity are significant influencing factors as well as the presence of rain, drizzle or fog at the critical moment. The water film has a very high conductivity and causes a large voltage to be impressed across air gaps and the development of these arcs can lead to flashover.

In any case, leakage current illustrates the experienced surface activity which in turn is strongly linked with pollution and surface condition. Therefore, leakage current measurements are widely used worldwide as a tool to monitor and investigate site pollution, surface and material condition, surface electrical activity and overall performance of insulators of several different designs and materials, both in field and lab conditions. Specimens (rods and plates) are also used by researchers in order to focus on specific phenomena of surface activity or the performance of materials without being influenced by the insulator design. The scope of this paper is to review leakage current monitoring conducted by different researchers worldwide primarily in respect to the variety of applications, the waveform shapes recorded, the techniques applied on LC waveforms, the extracted values and the derived conclusions concerning the experienced electrical activity and use of LC measurements.

## 2. BASIC LAB TESTS FOR INSULATORS

Laboratory tests are performed in order to provide a comparison of different insulator types and materials, a view of the performance of insulators under different conditions and to investigate the behavior of materials under certain types of stresses. Further, they can also be conducted in order to test the insulators' withstand on severe stressing or to a worst case scenario which can be decided according to the pollution severity of the installation site [1].

The four basic standardized tests that researchers usually follow are the salt-fog test [5], the clean-fog or solid-layer test [5], the inclined-plane test [6] and the rotating-wheel-dip test [7]. Researchers also facilitate custom variations of these or employ different tests, even non-standardized ones, in order to investigate phenomena of interest. A different category includes ice tests [3] employed in order to investigate the insulations' performance during ice accretion.

### 2.1. Inclined-plane test

The inclined-plane test is conducted in order to investigate resistance to tracking and erosion. Plate

samples are generally used in the inclined plane test. During inclined-plane test, the plate specimen is drilled and electrodes are attached. Then, the specimen is washed with a suitable solvent, rinsed with distilled water and mounted at certain angle (proposed: 45 degrees). A contaminant of certain composition and resistivity is allowed to flow, at a certain flow rate, from high voltage (higher) to ground (lower) electrode. With the contaminant flowing uniformly, voltage is applied on the specimen and timing starts until tracking is observed (or after 6 hours have passed). During this test, leakage current flows through the conductive path formed by the flow of the contaminant and may cause partial evaporation of the contaminant, formation of dry bands and arcing.

## 2.2. Rotating wheel dip test (RWDT)

The rotating-wheel-dip test, sometimes referred to as the merry-go-round test, has been used as an alternative method to evaluate resistance to erosion and tracking. In this method, the tested cylindrical specimens are fixed on a rotating wheel and are turned around continuously, dipped to salted water and then exposed to high voltage. The specimens are cleaned before mounting, using de-ionized water. They are mounted at an angle of 90$^{o}$ from each other and rotated at a steady speed (it is proposed that a full cycle should take 32 seconds). The second part of the cycle (after the dipping) permits the excess saline solution to drip off the specimen ensuring that the light wetting of the surface gives rise to sparking across dry bands that will form during the third part of the cycle (voltage application). In the fourth part, the specimen surface that had been heated by the dry band sparking is allowed to cool.

## 2.3. Salt-fog test

The salt fog tests are conducted in specially designed salt-fog chambers. The tested insulator or specimen is put in the chamber and salt-fog is used as an artificial pollutant. This procedure simulates coastal pollution where a thin conductive layer, formed by salt, covers the insulator surface. In practice, this layer contains little –if any- insoluble material. The salinity is measured usually by measuring conductivity or by measuring the salt density with a correction of temperature. The fog is produced in the test chamber by sprays and the solution is atomized by a stream of compressed air, flowing at certain angles to the solution nozzle. The test starts while the cleaned insulator is completely wet. The insulator is energized, the salt-solution pump and air compressors are switched on and the test is deemed to have started as soon as the compressed air has reached the normal operating pressure. If the insulator does not flashover after 20 min, the voltage is raised in steps of 10% of the test voltage every 5 min until flashover. After flashover the voltage is re-applied and raised quickly as possible to 90% of the previously obtained flashover voltage and thereafter increased in steps of 5% of the initial flashover voltage until flashover. The last process is repeated six times. After the eighth flashover, the fog is cleared and the insulator is cleaned. The next stage is called “withstand test”. A series of tests are performed on the insulator at the specified test voltage using a salt solution having the specified test salinity. The duration of each test is 1 h or until flashover. The insulator is washed before each test. The acceptance criterion for the withstand test is that no flashover occurs during a series of three consecutive tests. If only one flashover occurs, a fourth test shall be performed and the insulator passes the test if no flashover occurs.

## 2.4. Solid layer test (Clean-fog test)

During the solid-layer test, the insulators or specimens are artificially contaminated prior to exposure to a clean fog. This procedure simulates pollution conditions with thicker layers of deposits containing binding materials and some kind of salt. A slurry usually made of Kaolin, NaCl, and water is used as contaminant. The layer is left to dry before entering the clean fog chamber. The fog generators should provide a uniform fog distribution over the whole length and around the test object. A plastic tent can also been used, surrounding the test object, to limit the volume of the chamber. Two different procedures are proposed in order to test the pre-contaminated objects in the clean-fog chamber. During Procedure-A the wetting is performed before and during energization and the tested insulator is dried and re-tested whereas during Procedure-B the wetting is performed after energization. Procedure-A is rarely used and is not considered to be optimal. Procedure-B is usually preferred [3]. The overall procedure is different in each case and detailed description can be found in [5].

## 2.5. Ice tests

Several tests procedures for insulators covered with ice and snow are also conducted [3]. Most of the techniques use some kind of nozzle for ice accre-

tion on energized or non-energized insulators, and wind generation systems are sometimes also used. The voltage should already be applied during the ice accretion. Reference parameters include the time duration of the icing period, the length of the formatted icicles, the weight of the ice deposit on the insulator, the thickness of the accumulated ice on monitoring pipe or conductor exposed to the same icing conditions as those of the test object. A single constant voltage test is usually performed since voltage application results to surface heating and ice melting. The test ends if a flashover occurs or if the probability of a flashover is judged to be low. Tests may then be repeated with renewed snow covering and higher or lower voltage. In most cases the aim is to determine the withstand voltage of the insulator under certain icing conditions. In this case, the ice accretion is stopped after reaching the specified value and the test voltage is then applied. Generally, activity evolves as described in paragraph 1. Leakage current flows through the contaminated surface and dry band formation and arcing occurs which may lead to flashover.

## 3. MEASURING LEAKAGE CURRENT IN THE LAB AND IN THE FIELD

Laboratory tests offer valuable information but can not reproduce exact field conditions. Further, especially in the case of hydrophobic insulators, local conditions (weather, environment, resting time etc) strongly affect the overall performance of insulators. Field measurements on the other hand provide an exact view of the insulators' performance in the field but are much more demanding and require long term monitoring in order to be conclusive. Field measurements can be conducted in insulators that are part of the grid or isolated and a guide for the design of open air insulator test stations has been published [8].

Leakage current monitoring has been applied on a number of lab tests. It should be noted that it is not unusual for researchers to create their own variations and tests in order to serve their purposes. Grouping all similar tests to the same general category related to experimental arrangements results to Table 1 which portrays the various different tests employed in [9-63]. As shown in Table 1, leakage current has been measured during salt-fog tests [9-26], clean-fog tests [11,27-35], inclined-plane tests [36-39,60], rotating-wheel-dip tests [40-43], ice tests [56-58] and on various field installation sites [9, 19, 30,44-54,63]. Leakage current monitoring has also been conducted in test variations employing a pollution chamber [55], employing the "flow on" method which is a variation of the solid-layer test [59] or employing a variation of the inclined plane test to study the effect of length compression [60]. Leakage current has also been monitored on plate samples to study the effect of scattered droplets on leakage current and on the electric field [61] or to investigate the effect of non-uniform pollution which was acquired by spraying a glass plate sample using a can [62].

Field measurements have been conducted in environments characterized by the researchers as marine/coastal [44-46,53-54], tropical [11], industrial [9,11], desert [9], inland [19], and agricultural/rural [9]. Field measurements have been performed on insulators tested at specially designed test stations [45,46,51] or on insulators that are part of the grid and are installed either in transmission or distribution lines [9, 30, 48-50] or substations (post insulators) [44,53-54,63]. Also measurements have been conducted on energized but isolated rods installed at test sites [19] and energized but isolated insulators that are exposed in natural pollution [47]. A combination of field and lab tests has sometimes been used with field aged insulators that are tested in the laboratory [9,11,24,26,27] or pre-contaminated insulators tested in field conditions [47].

### 3.1. Measuring leakage current on different insulators types

Leakage current monitoring has been employed on insulators of various types. Measurements have been conducted on single suspension insulators of various designs [10,11,22-28,31,33,35,43,45-46], on dead-end insulators [12], on several line-post insulators with and without creepage extenders [18], on post insulators [44,47,51,53,54,56,58,63], on arresters [43], on distribution insulators of different designs [21] and even on insulator type specimens with a single straight shed [57]. Also on insulators of flat (aerodynamic) [9,52], antipollution [32], fog [52] and superfog [52] profile, and on insulator strings [9,30,32,34,48-50] or on couples of cap and pin insulators [27,29].

### 3.2. Measuring leakage current on insulators of different materials

Measurements have been conducted on insulators made of various hydrophilic and hydrophobic materials and also on hydrophilic insulators that have been coated with hydrophobic coatings. Hydrophylic insulators (porcelain and glass) are often described

**Table 1.** Leakage current measuring on different tests and materials.

| Table 1-A | Ref: —> | 9 | 10 | 11 | 12 | 13 | 14 | 15 | 16 | 17 | 18 | 19 | 20 | 21 | 22 | 23 |
|---|---|---|---|---|---|---|---|---|---|---|---|---|---|---|---|---|
| Installation | Salt-fog | S | I | P,R | I | I,P,R | P | R | R | R | I | R | I,R | I | I | I |
| | Clean-fog | S | I | I,P,R | | | | | | | I | | | | | |
| | Field* | S | | | | | | | | | | | | | | |
| Material | RTV | | | P | | R | P | R | | R | | R | R | | | |
| | HTV | | | P,R | | P,R | | R | R | | | R | R | | I | |
| | LSR | | | | | | | | | | | | | | | |
| | RTV coat. | | | I | | | | | | | | | | | | |
| | SIR | | | I | I | | | | | | I | | | I | | |
| | EPDM | | | I | | | | | | | | | | | | |
| | Non-ceramic | | | | | | | | | | I | | I | | | |
| | Glass | | | | | | | | | | | | | | | |
| | porcelain | S | | I | | | | | | | I | R | | | | |
| | Ceramic | | I | | | | | | R | | | | | | | I |

S = String, I = Insulator, R = Rod, P = Plate
*Field denotes LC measurements in the field (not just field aging)
**RWDT=Rotating-Wheel-Dip Test

| Table 1-B | Ref: —> | 24 | 25 | 26 | 27 | 28 | 29 | 30 | 31 | 32 | 33 | 34 | 35 | 36 | 37 | 38 | 39 |
|---|---|---|---|---|---|---|---|---|---|---|---|---|---|---|---|---|---|
| Installation | Salt-fog | I | I,R | I | | | | | | | | | | | | | |
| | Clean-fog | | | I | I | I | I | S | I | S | I | S | I | | | | |
| | Inclined-plane | | | | | | | | | | | | | P | P | P | P |
| | Field* | | | | | | | S | | | | | | | | | |
| Material | RTV | | R | | | | | | | | | | | | | | |
| | HTV | | R,I | I | | | | | | | | | | P | | | |
| | LSR | | | I | | | | | | | | | | | | | |
| | Hybrid | | | I | | | | | | | | | | | | | |
| | SIR | | | | | | | | I | | I | | | | | P | P |
| | Polyester resin | | | | | | | | | | | | | | P | | |
| | Non ceramic | | | | I | | | | | | | | | | | | |
| | Glass | I | | | I | | | | | | | S | | | | | |
| | porcelain | | R | I | I | | | | I | S | | S | | | | | |
| | Ceramic | | | I | | I | I | S | | | | | I | | | | |
| | Semiconducting | | | I | | | | | | | | | | | | | |

S = String, I = Insulator, R = Rod, P = Plate

*Field denotes LC measurements in the field (not just field aging)

**RWDT=Rotating-Wheel-Dip Test

| Table 1-C | Ref: —> | 40 | 41 | 42 | 43 | 44 | 45 | 46 | 47 | 48 | 49 | 50 | 51 | 52 | 53 | 54 | 55 |
|---|---|---|---|---|---|---|---|---|---|---|---|---|---|---|---|---|---|
| Installation | Salt-fog | | R | | R | | | | | | | | | | | | |
| | Pollution chamber | | | | | | | | | | | | | | | I | |
| | Solid layer | | | | | | | | I | | | | | | | | |
| | RWDT*** | R | R | R | R | | | | | | | | | | | | |
| | Field* | | | | | I | I | I | I | S | S | S | I,R | I | I | I | |
| Material | RTV | R | | R | | | I | | | | | | I | | | | |
| | HTV | R | | | | | | I | | | | | | | | | |
| | Hybrid | | | | | I | | | | | | | | | | | |
| | RTV coat. | | | | R, I | | | | | | | | | | I | I | I |
| | SIR | | R | | | | I | | | | | | | I | I | I | |
| | EPDM | R | R | | | | I | I | | | | | | I | | | |
| | Bisphenolic epoxy resin | R | | | R | | | | | | | | | | | | |
| | Cycloaliphatic epoxy | R | | | R | | I | | | | | | | | | | |
| | Acrylic | | | | R | | | | | | | | | | | | |
| | Non ceramic | | | | | | | | | | | | R | | | | |
| | Glass | | | | | | | I | | S | S | S | | I | | | |
| | Porcelain | | | | | I | I | | | | | | I,R | I | I | I | |
| | Ceramic | | | | I | | | | I | | | | | | | | |

S = String, I = Insulator, R = Rod, P = Plate

*Field denotes LC measurements in the field (not just field aging)

**RWDT=Rotating-Wheel-Dip Test

| Table 1-D | Ref: —> | 56 | 57 | 58 | 59 | 60 | 61 | 62 | 63 |
|---|---|---|---|---|---|---|---|---|---|
| Installation | Salt-fog | | | | | | P | | |
| | Inclined-plane | | | | | R | | | |
| | Ice chamber | I | I | I | | | | | |
| | Field* | | | | | | | | I |
| | Non-standard | | | | I | | | | |
| | Pollution slurry (flow on) | | | | | | | | |
| | Spraying with can | | | | | | | P | |
| Material | HTV | | I | | | | P | | |
| | SIR | | | | | R | | | |
| | Glass | | | | | | | P | |
| | porcelain | | | | R,I | | | | I |
| | Ceramic | I | | I | | | | | |

S = String, I = Insulator, R = Rod, P = Plate
*Field denotes LC measurements in the field (not just field aging)
**RWDT=Rotating-Wheel-Dip Test

as ceramic while hydrophobic materials are described as non-ceramic. Several hydrophobic materials are used for insulation, with the most usual being Room Temperature Vulcanized Silicone Rubber (RTV SIR), High Temperature Vulcanized Silicone Rubber (HTV SIR) and Ethylene Propylene Diene Monomer (EPDM). RTV SIR coatings are also employed on ceramic insulators to give them a hydrophobic surface.

Leakage current has been monitored on different insulators that were all made by a single material like porcelain [9,32,35,59,63], glass [24,49-50], SIR [12,21,33], HTV SIR [22,25] and RTV SIR coated insulators [55]. Measuring leakage current on a single insulator throughout the whole test has also been reported in case of ceramic insulators [23,28,29,56,58].

Measurements have also been conducted on groups of insulators of different materials. The interest is focused on the comparison of non-ceramic and ceramic materials and measurements on SIR [11,18,31,45,51-53], EPDM [11,45,46,52] and RTV SIR coated [11,43,53-54] insulators have been conducted along with measurements on porcelain [11,18,31,45,51-54] or glass insulators [26,46,52]. Leakage current on different insulators made by different non-ceramic materials has also been monitored in the case of SIR, EPDM and RTV SIR coating [11], HTV SIR and EPDM [46], SIR and EPDM [52] and SIR and RTV SIR coated [53-54]. In one case, LC on a hybrid insulator having SIR sheds and ceramic core and a porcelain semi-conducting glazed insulator has been monitored along with HTV SIR, LSR, glass and porcelain insulators [26].

It should be noted that the material is not always fully clarified by researchers with only the basic discrimination between hydrophobic or hydrophilic material being provided. The material of tested insulators in [9-63] is portrayed in Table 1 in reference to the employed test. Ceramic and non-ceramic categories in Table 1 include the non-clarified hydrophilic and hydrophobic materials correspondingly.

### 3.3. Measuring leakage current on specimens (samples) of different insulation materials

The specimens used are either cylindrical specimens, frequently referred to as rods, or plate specimens. In rotating-wheel-dip tests is custom to use cylindrical specimens, and measuring of the leakage current on those specimens is sometimes conducted [40-43]. Further, leakage current monitoring on cylindrical specimens (rods) has also been conducted during other tests [11,13,15-17,19,20,25,51,59-60]. By using rods, researchers obtain results that are not affected by the insulators' shape and therefore can investigate the materials' performance more accurately. A rod can be constructed or coated with the investigated mate-

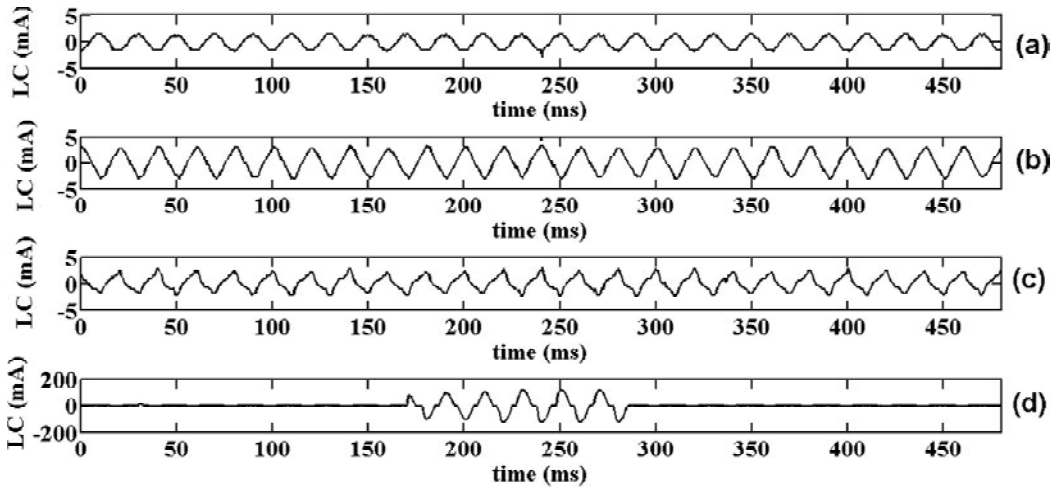


**Fig. 1.** An example of the basic waveform shapes: a. sinusoid, b-c. distorted sinusoids and d. arc/discharge.

rial (e.g. RTV SIR). The monitored rods are mainly made of non-ceramic materials such as RTV SIR [13,15,17,19,20,25,40,42] and HTV SIR [11,13,15,16,19,20,25,40]. Ceramic [16,19,25,51,59] or plastic [43] rods are sometimes included in research in order to offer a control element. In case of rotating-wheel-dip tests, leakage current on rods of other hydrophobic materials such as bisphenolic epoxy [40,43], cycloaliphatic epoxy [40,43] and EPDM [40,41] has also been measured.

Non-ceramic plate samples are mainly used in inclined plane test to investigate tracking and erosion, and such tests have also been combined with leakage current measurements [36-39]. Materials such as HTV SIR [36], polyester resin [37] and SIR [38-39] are used for plate samples. An HTV SIR plate sample has also been employed in a salt-fog test [13]. Plate samples have also been used in order to investigate the effect of different hydrophobicity levels in LC measurements. During one experiment, HTV SIR and RTV SIR plate samples were immersed in de-ionized water at 50 °C for different time periods in order to obtain different hydrophobicity levels, and then be tested in a salt fog chamber where leakage current was measured [11]. The electric field and the behavior of droplets on HTV SIR plate samples along with leakage current measurements have also been investigated [14,61].

Finally, a SIR rod sample has been employed, instead of a plate, on a variation of the inclined-plane test to study the effect of length compression on dry band arcing energy [60], and a glass plate sample has been employed to investigate the leakage current during non-uniform pollution conditions that were acquired by spraying non-uniformly the plate using a can [62]. Table 1 portrays the type of specimens employed in [9-63].

## 4. LEAKAGE CURRENT WAVEFORM SHAPERS AND CORRELATED SURFACE ACTIVITY

The basic stages of surface activity have been well correlated with certain leakage current waveform shapes. All researchers agree that the flow of current through a conductive film on the insulators surface results to sinusoid LC waveforms, whereas strong discharges (arcs) result to waveform shapes portraying a time-lag of current onset and a knee-like shape. As an intermediate stage, distorted sinusoids of various shapes occur. An example of typical waveform shapes is portrayed in Fig. 1.

It should also be noted that at the very early stages of activity, a sinusoid capacitive leakage current is recorded [11,12,18,20,35,56,58]. This current is minimal, in the area of μA, and refers to the insulators' behavior as a capacitor, and therefore it is often neglected during testing and monitoring.

The term "distorted waveforms" describes a large variety of waveform shapes. Some researches discriminate between less distorted (closer to pure sinusoid) and more distorted waveforms especially when they perform visual observations [13,28,30,31]. This is because the sharper tips of half-waves present on more heavily distorted waveforms, as the one in Fig. 1c, have been correlated with the occurrence of visible minor discharges whereas waveforms with a minor distortion similar to the one shown in Fig. 1b (often called triangular or sawtooth) have

been attributed to not visible faint discharges [28,34]. It should be noted that the chemical content of the pollutants can also play a role in the waveform shape of distorted sinusoids [33,64] and that the insulator's shape has also been reported to play a role in the way that activity advances [25,26]. Also that prior to the symmetrical discharge stage (Fig. 1d), pulses have been frequently reported to superimpose on the waveform crest. This is a stage reported by several but not all researchers. These pulses exhibit various amplitudes and they can be rather isolated or more frequent.

The appearance of large isolated pulses on the waveform crest has been reported in lab [10,15] and field measurements [54,65] and it has been correlated with the severity of the stress conditions [15] and the existence of high salt-density fog [10]. The mechanism is considered as follows [10]: the deposition of high salt-density fog to the contamination surface decreases the resistance rapidly, resulting in the increase of leakage current with strong discharges. This large current provides excessive extend of dry bands and prevent the occurring of successive discharges. On the other hand, clean fog doesn't decrease the surface resistance rapidly, resulting in the gradual development of dry bands and, as a result, discharges occur successively for several half waves.

Not as isolated but nevertheless intermittent and non-symmetrical pulses have also been reported to appear in several cases, as activity advances, prior to the appearance of arcs. Such pulses are reported to be the result of short strong discharges occurring before the more excessive discharges (arcs) that result to the symmetrical waveforms [10,13,16,18,19,25,28,30,31,34,44]. However, this is not recognized by all researchers as a separate stage. It should be noted that the presence, shape and movement of water droplets result to corona discharges which are illustrated in LC in the form of current peaks [14,16,17,25,38,61]. Visual inspections performed in some tests, showed that the smaller pulses (the shaper tips of distorted sinusoids) are the result of corona discharges [13,15-17] of bluish color [13,15], whereas larger pulses (symmetrical or not) are the result of discharges (arcs) which produce a yellowish to whitish color [13,15,28,30,31]. However, it should be noted that several small discharges may superimpose to produce a larger peak and that it is possible for a strong single discharge to last only for a half cycle. Therefore, a strict criterion has not been set in order to discriminate pulses' origin based on their amplitude or shape and it is not absolutely safe to conclude whether a pulse is the result of corona discharges or short arcing based only on the leakage current waveform shape, although the usual case should be considered to be that small tips of distorted sinusoids are the result of corona discharges while larger pulses are the result of (partial) arcing.

It should be noted that similar waveform shapes have been recorded during ice accretion tests [56-58]. In such cases distorted waveforms with sharper tips have been correlated to intermittent electric discharges at the tips of the icicles formed around the insulator sheds [56] or along the air gaps [58]. It has also been reported that these discharges have a bluish (violet) color [56, 58]. Symmetrical waveforms like the one shown in Fig. 1d [56-58] and pulse waveforms [57] have also been recorded and attributed to white partial arcs occurring as activity advances [56-58].

Finally, it should be noted that waveforms do not always correspond clearly to a certain stage. This may not be evident in accelerated lab tests, although the need of assigning each half-wave to a different component is often reported [13,16,19,25, 42], but becomes more obvious in case of leakage current waveform monitoring in the field [54, 65]. In the field, activity is not straight forward, surface conductivity may change rapidly or gradually, different parts of the insulator could be subjected to different conditions and surface condition may also vary from part to part. All these factors result to a variety of complex waveforms. A number of field waveforms, recorded in a coastal 150 kV high voltage substation suffering from sever marine pollution [44,53-54,65], are presented in Fig. 2 including typical and more complex waveform shapes.

## 5. LEAKAGE CURRENT AND OTHER FACTORS

Leakage current monitoring is often conducted along and correlated to other factors and values. In terms of electrical values, the applied electric stress is most usually monitored, especially when different levels of voltage are applied [11-12,14,15,18, 20,24,27,29,39,48,59,61,62]. Monitoring optical emissions [13], changes in the molecular structure of polymer materials [19, 25], e-field [14], flashover voltage [24,27,59] and phase angle between leakage current and applied voltage [24,31] has also been performed. Besides the basic values (contamination level, relative humidity, fog conductivity, air pressure, flow rate, aging time etc) which are measured as part of most test procedures, other parameters related to the pollution phenomenon such

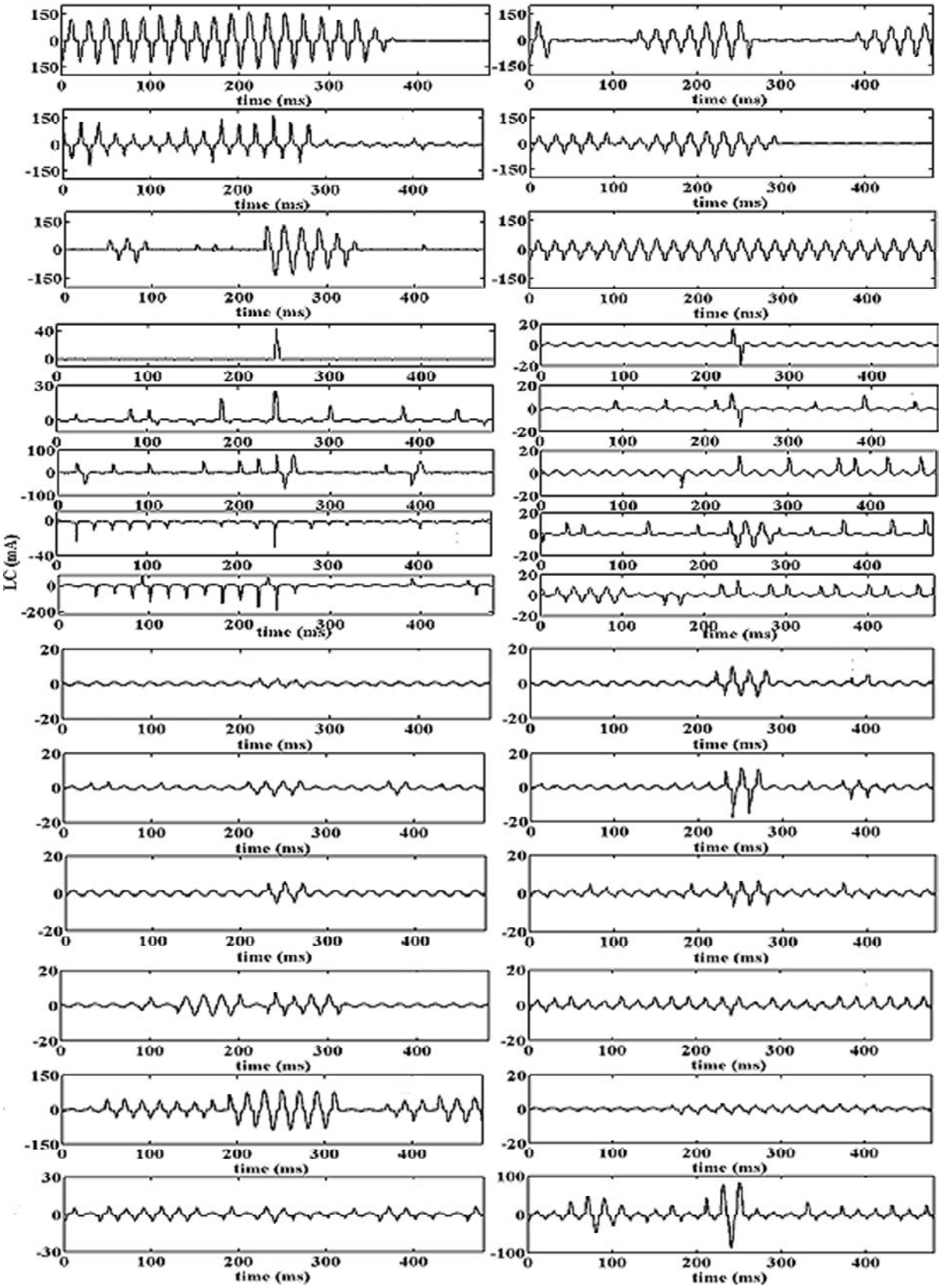


**Fig. 2.** Field waveforms.

as wetting time [9] and resting time [11] have also been monitored and correlated to leakage current measurements. Further, the behavior of water droplets on the surface (hydrophobicity class and contact angle measurements) is frequently monitored along with leakage current [14,16,17,25,38,61].

## 5.1. Signal analysis on leakage current measurements

A large number of signal analysis techniques has been proposed and applied on leakage current measurements and several values have been extracted from leakage current measurements using these techniques. A general categorization is applied on this paper depending on the followed procedure and the values extracted.

Six basic categories are defined:

**I.** The calculation of basic electrical values such as bin counting, peak rate, surface resistance, V-I plots and characteristic, peak value, cumulated charge, flashover voltage and LC amplitude in last half cycle before flashover.

**II.** Advanced analysis techniques, primarily in the time domain, employed on LC waveforms such as the differential technique, the correlation and autocorrelation function, the similarity function, the moving average and the envelope of leakage current.

**III.** The separation of leakage current waveforms in different components related to surface activity such as: conductive component, dry band arc component and partial discharge component or sinusoidal component, local arc component and transition component or conductive component and dry band arc component.

**IV.** The frequency analysis of leakage current which includes monitoring the frequency content, the power spectrum, the harmonic content, the ratio of different harmonic contents and the total harmonic ratio. Frequency analysis is usually performed using Fourier Transforms but Auto Regressive analysis and Wavelet analysis have also been employed.

**V.** The employment of pattern recognition on LC measurements with techniques and tools such as Artificial Neural Networks, Statistical Pattern Recognition and Recurrent Plot Analysis.

**VI.** The employment of the STD_MRA technique which is a pattern extraction and frequency analysis technique that uses standard deviation of the details derived in each level of the Multiresolution Analysis performed with wavelets.

## 5.2. Electric values

### 5.2.1. Peak value recording and bin counting

The most usual measurements [3] concerning leakage current are: the monitoring of peak leakage current value during given time periods and counting the number of pulses that exceeds given thresholds, a technique frequently called bin counting.

Bin counting has been employed by various researchers [9,36,50,52,55]. It is a technique most commonly used in the field due to the small amount of recorded data required [3]. Using this technique researchers obtain a rough map of the insulators performance and minimize the amount of recorded data which is rather important in case of long term and/or field monitoring. For example, if one chooses to set 4 levels then regardless the monitoring period, only four values per insulator will be recorded. However, the actual value of the peak current is lost and therefore a difference in behavior that result to peak values of the same level, will also be lost. In case of field measurements, Fierro-Chavez et al. [9] defined 5 different levels for leakage current measured on insulator strings (mA: 50~150, 150~250, 250~350, 350~450, >450). A similar research by Montoya et al. [52] employed 6 different levels (mA: <50, 50~150, 150~250, 250~350, 350~450, >450). Oliveira et al. [50] applied bin counting in the non-sinusoid component of the current employing 3 different levels (mA: 5~10, 10~20, >20). In case of lab tests, Devendranath et al. [55] applied bin counting during a pollution chamber test employing 8 levels (mA: 0~50, 50~100, 100~200, 200~480, 480~580, 580~680, 680~780, 780~880), whereas Kim et al. [36] used the same technique during an inclined-plane test and defined 4 levels of activity (mA: 1~10, 10~30, 30~50, >50).

Recording the actual peak leakage current value provides a more detailed investigation than bin counting, although it results to significantly larger amount of data. Peak value monitoring means that instead of counting the number of surges that exceeds different thresholds, one can measure the actual minimum and/or maximum value in predefined time intervals e.g. in each cycle [41], in each 200ms [10], every 30 seconds [26], every 10 minutes [46], every day [51] or even during a single RWDT rotation [42] or long term RWDT [40,41,43]. Monitoring the temporal variation of leakage current peaks in irregular or undefined time intervals has also been reported [11,26]. In addition, monitoring the peak value of different frequency components has also been employed [20,28,30,33].

### 5.2.2. Cumulated charge, V-I characteristic and others

Cumulative charge is probably the next frequently used value, employed in a variety of tests [13,25,41-

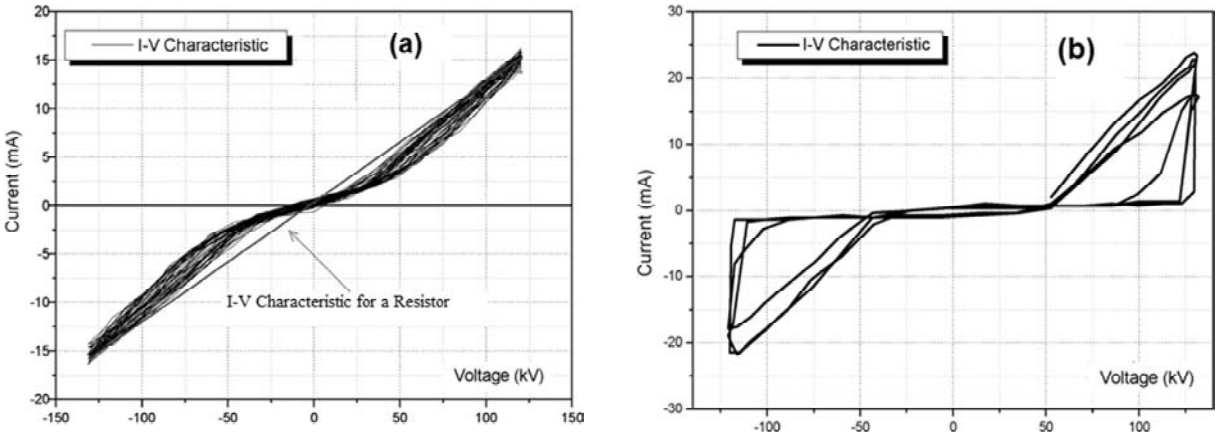


**Fig. 3.** I-V characteristic in case of (a) a distorted sinusoid LC waveform (similar to Figs. 1b-1c) and (b) a symmetrical distorted waveform with time lag of current onset (similar to Fig. 1d).

44,46] and even calculated for different leakage current components [13,16,19,22,25,42].

Cumulative charge is represented by the area between the LC waveform and the horizontal time-axis and is given by

$$Q = \int_0^T |i(t)| \, \mathrm{d}t,$$

where $i(t)$ is the instantaneous value of the leakage current and $T$ the monitoring period.

Other values usually monitored are the RMS value [10,11,36] and average values of leakage current [11,12,55]. Values such as the maximum and mean apparent charge per cycle [12], variation of mean and maximum values of LC and standard deviation [32,34], the amplitude of the LC in the last half cycle before flashover [27], the peak rate [48], V-I plots [18,29] and I-V characteristic [63] have also been investigated.

All these values give an indication about the magnitude of the LC waveform but are not linked with the waveform shape and, thus, with the type of activity, with the exception of the I-V characteristic. At the initial stage of activity when sinusoids and distorted sinusoids are recorded, the I-V characteristic is nearly linear indicating a resistive surface behavior as shown in Fig. 3a. As activity advances and leakage current becomes more distorted the characteristic changes illustrating a hysteresis effect as shown in Fig. 3b.

## 5.3. Advanced analysis

Several analysis techniques have been applied on leakage current waveforms. Techniques that are related to the time-domain signal but are not basic, are described in this paper with the term “advanced”. A mathematical basis for each technique, when required, is given in Table 2.

Otsubo et al. [13] used a differential technique to identify arcs. A large rate of change in the leakage current was correlated to arc ignition. When the differential value of current became larger than a threshold value (which was set as 5 times the averaged differential value) then an arc ignition was assumed.

El-Hag [20] used the autocorrelation function (ACF) in 120 min intervals of LC measurements in order to detect non-randomness in recorded data. The author calculated up to the 16$^{th}$ lag number with 97.5% confidence limit (see Table 2A).

Homma et al. [42] introduced the “Similarity, *S*” function in order to characterise the waveform distortion. The parameter *S* is defined as the ratio of time integrated leakage current over a half cycle to the time integral of a sine wave of amplitude corresponding to the peak value of the measured leakage current (see Table 2B).

Sarathi et al. [38] used a moving average technique in order to obtain a clear trend of the data. The basic understanding of a moving average is that it is the average magnitude of current at a specific point of time. By creating an average magnitude of the current that moves with the addition of new data, the characteristic variation is smoothed out so that the fluctuations with time are reduced and what remains is the stronger indication of the trend in the variation of leakage current magnitude over the analyzed period. The authors used a simple moving average technique (see Table 2C). In their paper a 240 point window frame was used.

**Table 2.** Mathematical basis for advanced analysis techniques discussed in paragraph 5.3.

| A. Auto Correlation Function | B. Similarity |
|---|---|
| Given the measurements $Y_1$, $Y_2$,..., $Y_N$ at time $X_1$, $X_2$, ..., $X_N$ the ACF for the lag number $k(r_k)$ is given by the following equation: $$r_k = \frac{\sum_{i=1}^{N-K}(Y_i - \overline{Y})(Y_{i+k} - \overline{Y})}{\sum_{i=1}^{N}(Y_i - \overline{Y})^2}$$ | $$S = \frac{\int_0^{\pi/\omega} I(t)\,\mathrm{d}t}{\int_0^{\pi/\omega} I_0 \cdot \sin(\omega t)\,\mathrm{d}t}$$ where $\omega = 2\pi f$, $f$: frequency, $t$: time. |
| **C. moving average technique** | **D. moving average technique** |
| A window consisting of $k$ points was chosen to find the moving average using the formula: $$X_i = \frac{\sum_{N=i}^{N=i+k} Y_N}{k}$$ where $X_i$ are the newly calculated moving average points corresponding to $Y_N$ raw data points. | The smoothen point being was plotted calculated using the formula: $$Y_{sm} = \frac{A\nu_1 + A\nu_2}{2}$$ where $Y_{sm}$ is a smoothen point, $Av_1$ the average of the first half of window width and $Av_2$ the average of the second half of window width. |
| **E. Leakage Current Envelope** | |
| The Hilbert transform given by $$\overline{i} = H\{i(t)\} = \frac{1}{\pi}\int_{-\infty}^{\infty}\frac{i(t)}{t-\tau}\,\mathrm{d}t = \frac{1}{\pi}i(t) \otimes \frac{1}{t}$$ where $\otimes$ denotes convolution. The equation describing the envelope is given by $$i_a(t) = i(t) + j\,\overline{i}\,(t) \quad \text{and} \quad i_{env}(t) = |i_a(t)| = \sqrt{i(t)^2 + \overline{i}\,(t)^2}.$$ | |

Meyer et al. [39] also used a moving average technique to smooth LC data (see Table 2D). The window width was kept to 1% of total number of points which was 14400 for each graph corresponding to 4 hours of testing. The moving average technique was also used by Lopes et al. [12] to show the trend of recorded mean and maximum apparent charge data using a 5-minute window and by El-Hag et al. [21] in order to portray the trend of leakage current RMS value.

The leakage current envelope is a technique that has been used [56,58,66] to portray an image of the leakage current behavior. The envelope can be calculated using the Hilbert transform [66] (see Table 2E). A more practical algorithm for calculating the Hilbert transform using Fourier transform is also described in [66]. Meghnefi et al. [56] monitored the evolution of the LC envelope whereas Amarh et al. [66] used the envelope to calculate the mean distance between successive crossings of a predefined threshold by the envelope, the time spent above threshold and the levels and frequency of large excursions of the envelope. Volat et al. [58] used the LC envelope to investigate the occurrence frequency evolution of electric discharges.

## 5.4. Separate components

It has been proposed that different parts (usually half-cycles) of the leakage current waveform could be attributed to different components and investigation could be conducted on the behavior of these components.

Homma et al. [42] proposed the use of the "Similarity, $S$" function to attribute each half cycle of the

recorded current to a conductive (sinusoid) or dry band arc component. The peak value of the current was detected in each half cycle and defined as the amplitude of an assumed sine wave. The mathematical parameter S was calculated from comparison between the time integral of actual current and the assumed sine wave. If the calculated parameter was found smaller than a threshold value, then the half wave was assigned to dry band arc component and if found larger than the threshold then it was assigned to conductive component.

Otsubo et al. [13] separated the leakage current into three components: conductive current, dry band arc discharge, and corona discharge current and calculated the respective cumulated charges. He used frequency content to identify corona discharge current and the differential technique to identify dry band arcs. The part that was not attributed either to corona or dry band arc, was considered conductive. Marungsri et al. [25] also reported similar research by separating leakage current in high frequency component (corona) and conductive and dry band arc component.

Kumagai et al. [16,19] employed wavelet transform in order to assign each half-wave of the recorded current to sinusoidal, local arc, and transition component. They attributed half waves exhibiting current onset time lag to local arcs and triangular-like half waves to transition between sinusoidal and local arc components. The assignment to a sinusoidal or a transition component was based on the distortion level of the half wave given by a ratio of third to first harmonic content calculated using wavelet transform. The assignment to local arc component was made by calculating the onset time of each half wave with the use of a sinusoidal half-wave with similar average value.

A different approach is the separation of components using the frequency domain, instead of the time domain, in order to monitor and investigate harmonic and frequency bands components, but since this is more a frequency analysis theme, it is further reviewed in the following paragraph.

## 5.5. Frequency analysis

### 5.5.1. Mathematical tools

Fourier analysis is mostly used by researchers to perform frequency analysis but the Auto Regressive (AR) analysis [10,34] and wavelet analysis [16,22,23,57] have also been employed. The mathematical basis for Fourier analysis is not presented in this paper, as it is a well known method. A short basis for AR and wavelet analysis is given below, but a more detailed review of the mathematical basis for frequency analysis techniques is out of this papers' topic and aim. In the AR model, all signals researched are regarded as the output when a white noise sequence $w(n)$ energizes a reversible cause-and-effect linear system [34]. The output sequence $x(n)$ can be expressed as

$$x(n) = -\sum_{k=1}^{p} a_k x\left(n-k\right) + w(k),$$

where $a_1,a_2,\ldots..,a_p$ are the AR model parameters.

Based on the theory of stationary random signals through linear systems the power spectrum of the output sequence $x(n)$ is given by:

$$P_x(w) = \frac{\sigma^2}{\left|1+\sum \alpha_\kappa \exp(-jwk)\right|},$$

where $\sigma^2$ is the variance of the white noise sequence. All the parameters of the AR modes including $\sigma^2$ and $a_1,a_2,\ldots..,a_p$ can be obtained by various algorithms.

The $p$+1 parameters ($a_1,a_2,\ldots..,a_p$) of a $p$-order AR model can compose a $p$-order linear prediction model and the minimum prediction error of the linear predictor is equal to the variance of the white noise sequence of an AR model, namely $\rho_{min}= \sigma^2$.

Wavelet analysis allows simultaneous time and frequency analysis of signals. A wavelet function is an oscillatory function, with an average value of zero and a band-pass like spectrum. The basic concept in wavelet analysis is to select an appropriate wavelet function $\Psi$ (the mother wavelet) and then perform the analysis of a signal using translated (shifted) and scaled (dilated) versions of the mother wavelet. The continuous wavelet transform is given by

$$W(a,b) = \left\langle f, \Psi_{a,b} \right\rangle = \int_{-\infty}^{\infty} f(t)\Psi_{a,b}(t)\,\mathrm{d}t =$$

$$\frac{1}{\sqrt{a}} \int_{-\infty}^{\infty} f(t)\Psi^*\left(\frac{t-b}{a}\right)\mathrm{d}t,$$

where $a$ represents the scale, $b$ represents the position, and $\Psi^*$ represents the complex conjugate of $\Psi$. The chosen mother wavelet should be a decaying oscillation function. The modulus and the phase of complex $W(a,b)$ correspond to the time-frequence information and the localized amplitude regarding the current in the cycle $a$ vicinity in time $b$.

In case a digitized signal and discrete values of $a$ and $b$ are used then the Discrete Wavelet Transform is given by

$$DWT(f,j,b) = \frac{1}{\sqrt{s_0^j}} \int_{-\infty}^{\infty} f(t)\Psi\left(\frac{t - k \cdot s_0^j}{s_0^j}\right),$$

where $a = s_0^j$, $b = ka = ks_0^j$ and $k,j \in Z$.

### 5.5.2. Frequency analysis application

Frequency analysis is frequently employed to investigate leakage current measurements since the frequency content is correlated not only with the leakage current amplitude but also with the shape of leakage current waveforms. The behavior of the frequency content as leakage current passes through various stages of activity has been thoroughly investigated [9,10,14,15,21,24,26,28,30, 52,57,63].

Frequency analysis has also been employed in order to separate components as reported in paragraph 6.4, and to investigate the content of different harmonics [20,21,23,24,28,30,33,37,39,47,58] or frequency bands [22,23].

The behavior of the ratio of the contents of different harmonics (e.g. third to fifth [24], fifth to third [33], third to first [36] ) and the Total Harmonic Distortion (THD) ratio [24, 35] have also been investigated.

The THD ratio is defined [35] as the ratio

$$THD = \frac{\sqrt{\sum_{n=2}^{\infty} I_n^2}}{I_1},$$

where $I_n$ is the $n^{th}$ order harmonic.

A fundamental frequency criterion has been applied in order to remove noise generated waveforms in case of long term field monitoring [53]. The behavior of the power spectrum over time has also been investigated [34]. Frequency analysis has also been employed during preliminary tests in case of designing a field monitoring system in order to decide upon the bandwidth and sampling rate [9].

## 5.6. Pattern recognition

### 5.6.1. Use of statistical pattern recognition

Lopes et al. [12] employed statistical pattern recognition to investigate the changes on the insulator surface and the observed transition from corona from water droplets to dry-band arcing. The measured mean and maximum apparent charges were used to create patterns. The nearest neighbor rule was used as a clustering technique in order to split the data in two parts, the discharges from water droplets (first cluster) and the dry-band arcs (second cluster). With the clusters defined the mean and standard deviation of each data set were obtained, and the unit standard deviation contours were plotted for both clusters. The goal of the classifier was to divide the maximum versus mean space used into regions separated by a discriminant boundary. In the final step, the discriminant boundary was obtained using the Maximum a Posteriori Probability decision rule which take into account the position, shape and number of samples in each cluster, approximated by Gaussian distributions.

### 5.6.2. Use of recurrent plot analysis

Recurrent Plot (RP) analysis visualizes the degree of aperiodicity of time series in an m dimensional phase space. The non-linear characteristics of dynamic courses within signals can be illustrated on a map, which is composed of visible rectangular block structures with higher density of points. If the texture of pattern within such a block is homogeneous, stationarity is assumed for the given signal within the corresponding time period.

The RP is formed by comparing all embedded vectors with each other and drawing points when the distance between two vectors is below the threshold. Such a RP method can be mathematically expressed as

$$R_{i,j} = H\left(\varepsilon - \left\| X_{(i)} - X_{(j)} \right\|\right),$$

$$X_{(i)}, X_{(j)} \in R^m, \quad i,j \in (1,M),$$

where $\varepsilon$ is the predefined threshod; $H(x)$ is the Heaviside function; m is the embedding dimension; $X_{(i)} = [x(t_i), x(t_{i+\delta}), x(t_{i+2\delta}), \ldots, x(t_{i+(m-1)\delta})]$ $(j=0,1,2,\ldots,M)$ are vectors reconstructed from the sampled time series $x(t_j) = x(t_0 + j\Delta t)$ $(j = 1,2,3,\ldots,N)$; $\Delta t$ is the sampling time; $M$ is the total number of $X_{(i)}$ and $N$ is the length of the time series.

Du et al. [23,57] employed RP to extract graphical patterns from various frequency components of leakage current waveforms. They defined three different stages of activity (initial stage, intermediate stage and Just Prior to Flashover stage) and they proposed that the RP of high frequency components could be used as a pattern to identify each stage, and especially the latter one. In order to quantitatively describe the characteristic of RP, the recurrent rate (RR) and determinism (DET) were calculated. RR denotes the degree of nearness for the vectors in the phase space. DET differentiates the

recurrent plots connected with each other in the diagonial direction from the isolated recurrent point in a RP map. A smaller DET value denotes that the investigated system has less deterministic ingredient.

### 5.6.3. Use of artificial neural networks (ANNs)

Fernando and Gubanski [11] used ANNs to perform pattern recognition of leakage current waveforms. Two ANN were used in order to evaluated harmonic content (third and fifth harmonics) and a third one to classify the waveforms as sinusoidal, nonlinear or containing transients from discharges. In order to eliminate the problem of different LC levels, they normalized all waveforms by dividing the actual value with the maximum value. In order to evaluate harmonic content two 2-25-4 ANN were employed. After the normalization, the two inputs were obtained as the average value of two quarters of a positive half-cycle of LC waveform. A relationship between the output of the ANN and the content of third and fifth harmonic was proposed. In order to classify waveforms, a 2-15-3 ANN was employed. Similar to the previous procedure, two average values of 25 different normalized LC patterns were used for the training.

Bashir and Ahmad [24] employed a slightly different technique to normalize data by using the formula:

$$I = I_{\min} + \left(I_{\max} - I_{\min}\right)\left[\frac{D - D_{\min}}{D_{\max} - D_{\min}}\right],$$

where $I$ is the normalized value of a single datum; $I_{\max}$ and $I_{\min}$ are the input range of the ANN (typically -1 to 1 or 0 to 1); $D$ is the input value for each datum; $D_{\min}$ and $D_{\max}$ are the minimum and maximum values of the input data. They used the content of odd order harmonics (first to seventh), the THD and the third to fifth harmonic content ratio as inputs to an 6-11-7-3 ANN that performed the classification to three different classes related to ageing (severe corrosion, mild corrosion, no corrosion).

Li et al. [34] used an ANN to estimate the severity of surface contamination by estimating the ESDD. They used a slight variation to calculate mean, maximum and standard deviation of leakage current [32] and they used those values as well as relative humidity (RH) and applied voltage as inputs to the ANN. They normalized the current values by using the formula:

$$\overline{x}_i = \frac{\left(x_i - x_{\min}\right)}{x_{\max} - x_{\min}},$$

where $x_{\min}$ and $x_{\max}$ are the minimum and maximum values of x.

El-Hag et al. [21] employed ANNs in order to predict the final value of the leakage current at the end of the early aging period. They used a Gaussian radial basis function (GRBF) ANN which was found to perform better than a feed forward ANN. The initial value and the slope for the LC at each 10 min during the first 5 h of salt-fog test were used as inputs.

Jiang et al. [35] employed ANNs to evaluate the safety condition of insulators. They used the peak value of leakage current, the phase difference between LC and applied voltage and the Total Harmonic Distortion (THD) ratio as inputs for the ANN. They employed an ANN with fuzzy outputs. Four fuzzy subsets were defined correlated to four different safety conditions (safe, light alarm, moderate alarm, serious alarm) which were correlated to different surface activity (no discharge, fragment small arc, continuous small arc, intense main arc).

Ugur et al. [37] employed ANNs to analyze surface tracking during an inclined plane test. They used a A/D board that performed sampling at 40 kHz and they performed a 2048 FFT which meant that the board returned information about input frequencies to $f_n$ = 20 kHz. The FFT represents the sampled signal *u(t)* in terms of data values which are periodic with $T = N$t where $N$ is the total sample number and t the time between samples. The $n^{th}$ harmonic has the frequency $f_n$ where $f_n = nF$ and $f_n = (n/N)/(1/\tau)$. In order to reduce the processing time only the first 60 frequency components of the FFT were used as inputs to the ANN.

Volat et al. [58] used a self organized map ANN to monitor leakage current of ice-covered insulators. They used the phase shift between the LC and the applied voltage and the content of the third and fifth harmonic as inputs to the ANN. The ANN generated an input equal to 1 if the LC cycle in progress contains a discharge and 0 in all other cases. They defined four different classes of LC waveforms and they also correlated them with visual observations. They also used the occurrence frequency of discharges during a second (60 cycles) to predict the establishment of the permanent regime, a precursor of flashover imminence. A second ANN was used in this case. The 60 inputs of this ANN represented the average maximum LC amplitude calculated for each value of partial arc occurrence frequency, which

**Table 3.** An example of frequency bands for different MRA levels when a sampling frequency of 2 kHz is applied.

| Decomposition level | Approximation | Details |
|---|---|---|
| 1 | 0~500 (Hz) | 500~1000 (Hz) |
| 2 | 0~250 (Hz) | 250~500 (Hz) |
| 3 | 0~125 (Hz) | 125~250 (Hz) |
| 4 | 0~62.5 (Hz) | 62.5~125 (Hz) |
| 5 | 0~31.25 (Hz) | 31.25~62.5 (Hz) |
| 6 | 0~15.625 (Hz) | 15.625~31.25 (Hz) |

varies from 1 to 60 for each sequence of one second.

## 5.7. The STD_MRA technique

The STD_MRA technique is based on wavelet multiresolution analysis. Multiresolution analysis (MRA) is a wavelet based filtering algorithm, which was created as a theoretical basis to represent signals that decompose in finer and finer detail. The main idea is to use wavelet analysis to decompose the original signal in two parts: the approximation, which contains the low-frequency part of the signal, and the details, which contains the high-frequency part. The first stage of decomposition will give the first level approximation ($a1$) which if decomposed will give the second level approximation ($a2$) and so on. Detail analysis is performed with a contracted, high frequency version of the mother wavelet, while approximation analysis is performed with a dilated, low frequency version of the same wavelet. The standard deviation for the details derived in each level of decomposition is calculated in order to acquire the STD_MRA VECTOR which can be used as a pattern for the waveform and also as a quick indication of frequency content. The frequency band for each level can be computed from the sampling frequency $f_s$. Starting from $f_s/2$, each decomposition cuts the band in two halves with approximation being the lower half and detail being the upper half. For example if a sampling frequency of 2 kHz is used as in [67] then the frequency bands will be those in Table 3. A schematic representation of the procedure is shown in Fig. 4.

Chandrasekar et al. [31] employed STD_MRA in 7 levels with a 5kHz sampling frequency, investigated the STD_MRA plot shape in correlation with the LC waveform shape, and proposed the distortion ratio (DR) given by:

$$DR = \frac{D3 + D4 + D5}{D6}$$

with D6 containing the frequency band 39~78kHz and ($D3$+$D4$+$D5$) containing the frequency band (312~156 kHz). They also monitored the behavior of high frequency STD_MRA components to detect arcing.

Sarathi et al. [38] employed STD_MRA in 10 levels and investigated the STD_MRA plots in order to correlate them with changes in the contact angle of the specimen and thus with changes in the hydrophobicity level of the insulation material.

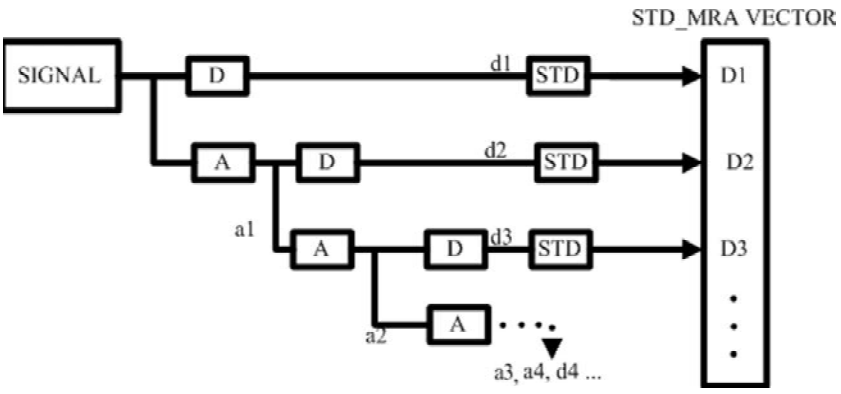


**Fig. 4.** A schematic representation of STD_MRA technique.

Pylarinos et al. [53] employed six level STD_MRA using a 2 kHz sampling frequency and proposed the $S_R$ ratio which is given by

$$S_R = \frac{D1}{D\max},$$

where $D1$ contains the frequency band 500~1000 Hz (see Table 3) and $D_{max}$ being the maximum value of the STD_MRA VECTOR. They proposed the use of $S_R$ as a measure of the impact of noise on field leakage current waveforms of small amplitude. They also proposed [67] that the STD_MRA VECTOR could be used as a pattern to train an ANN in order to automatically identify leakage current waveforms.

## 6. DISCUSSION

Leakage current monitoring is a well established tool to monitor surface activity and condition. It is a technique extensively used on insulators and specimens of various different materials and types. The basic phenomena of electrical activity have been well correlated with certain leakage current waveform shapes. However, identifying the phenomena taking place during the transition from one stage to another can be a more complex task.

It is well established that through continuously advancing activity, the magnitude of leakage current increases as it passes through different stages. That means that during an accelerated test, the magnitude of the sinusoid current will be smaller than that of the distorted sinusoid, which will in turn be smaller than an arc.

The general conclusion is that the levels of leakage current generally increase as the stress increases and as activity advances towards flashover. However, the type, shape and material of insulator along with local condition play a significant role and leakage current levels differ in case of different insulators and different conditions. Therefore, measurements on site on each different type of insulator have to be performed before such measurements can be used as perfomance indicators.

In addition, it is well established that although peak value of LC can be used as an indication it is not rather accurate since it can not be safely correlated to the waveform shape and, thus, to the type of surface activity. For example, El-Hag et al. [15] recorded, during the same test, dry bands that occurred with LC levels as low as 1mA whereas sinusoids of amplitude that reached 23 mA were also recorded. It should be noted that , as correctly mentioned in [10], it is impossible to obtain the exact same waveforms of leakage current even under the same general test conditions since the behavior of discharges, such as occurrence, elongation and extinction varies with wet conditions of the contamination layer every moment. Further, a criterion related to peak values can not be applied when conditions change (for example in case of different tests). This is a significant problem also in case of field monitoring where conditions change in a constant and chaotic manner. For example, Pylarinos et al. [54,65] showed that during long term field monitoring, waveforms of different types correlated to different surface activity can portray similar peak LC values. They recorded pure sinusoids with peak values as high as 29 mA, distorted sinusoid with peak values as high as 49 mA, intermittent pulses with peak values from 5 mA to 100 mA and discharges with peak values from 5 mA to 150 mA. Further, the presence of peaks due to field noise [53] can result to faulty alarming peak LC values.

The calculation and use of accumulated charge as an indication is frequently proposed as a more representative value. In fact, a high value of cumulative charge means that the recorded leakage current is generally high (therefore, it can be more reliable than peak related values). However, cumulative charge can not identify the shape of the waveform, which is connected to the type of activity. This is a matter of concern since local discharges and arcs inflict localized stress which can cause degradation of insulating performance and ageing especially in the case of polymer materials [10,13-14,16,24-25,36,39,60]. Therefore discharges are more dangerous than sinusoids of the same amplitude, although the cumulative charge (and peak related values) will be similar in both cases. This a common problem of most values mentioned in paragraph 5.1 with the exception of the V-I characteristic which can offer information for the waveform shape, although this information is not easily measured and interpreted numerically. More complex techniques have also been proposed, as described in paragraph 5.2, in order to obtain a clearer image of the LC behavior but they also suffer from most of the earlier mentioned disadvantages and, in their case, the increase of computation time and complexity is also an issue.

To cope with the problem several techniques have been proposed that offer a link with the waveform shape. Frequency analysis has shown that the odd-harmonic content increases as the waveform gets more distorted. This has been reported by all researchers as a general rule and, further, the behavior of different ratios of harmonic components (third to first, third to fifth, THD) have been proposed

as an indication of the distortion ratio. A similar approach has been conducted using wavelet analysis and the STD_MRA technique in order to obtain ratios related to the content of frequency bands. In this case, a correlation with the shape of LC waveforms has also been reported. However, although strong correlations have been reported, a universally accepted value and threshold is yet to be defined. Further, time allocation is lost during frequency analysis and different types of waveforms (e.g. waveforms portraying consequent and intermittent pulses) may exhibit the same frequency content.

Assigning different parts of the LC waveform (cycles or half cycles) to different components may seem a more accurate approach, however, one should note that the definition of the assignment criteria is a serious issue. For example, in case of the differential technique if the threshold is set too high then weak dry bands will not be included and if the threshold is set too low then halfcycles of distorted sinusoids could be regarded as arcs. In addition, such a technique can produce erroneous results in case of noise [53] and sudden amplitude changes that may occur when surface conductivity suddenly rises without the presence of arcs [54]. However, correlation of the behavior of different components to the waveforms' shape has been reported and it has been proposed that such parameters can also be used as an indication.

Pattern extraction and recognition techniques have shown good results in automating the identification and decision process but they have been employed on small sets of waveforms and a large scale application on field waveforms is yet to be performed. In addition, there is a large number of different values that has been used, and can potentially be used, as patterns and an even larger number of different techniques and topologies that can be applied. Further, surface activity during service and the resulting leakage current waveforms can be far more complex compared to waveforms recorded during lab tests or short-term field monitoring, due to the chaotic nature of field conditions. Therefore, further investigation and evaluation is required before applying pattern recognition techniques in the field during service.

## 7. CONCLUSION

Leakage current monitoring is a well established tool to monitor and investigate the insulators performance and surface activity which is linked with surface condition and electric and environmental stress experienced. This paper complements previous reviews on related topics [4,68,69] in terms that is focused on the large variety of applications of leakage current monitoring as well as on the large variety of the techniques applied on LC waveforms, the correlation of waveforms' shape and surface activity, the analysis techniques applied and the extracted values that have been proposed as an indication of the waveforms' shape and surface activity.

Leakage current measurements are performed on a variety of experiments conducted in the laboratory and in the field. They are performed on different types of insulators, on insulators made by different materials and also on insulator strings and on insulation samples such as rods and plates. They may even be performed on insulators during service conditions. A combination of field and lab tests has also been followed by some researchers with field aged insulators that are tested in the laboratory or pre-contaminated insulators tested in field conditions.

The basic stages of electrical activity have been well correlated with certain leakage current waveform shapes but identifying the phenomena taking place during the transition from one stage to another is a more complex task. The flow of resistive leakage current is correlated to sinusoid waveforms. As activity advances, the waveform becomes more distorted. Arcing results to symmetrical distorted waveforms of large magnitude that portray a time lag of current onset. Corona discharges can occur due to the presence and movement of water droplets on the surface. It is frequently reported that prior to distorted symmetrical waveforms (arcs), pulses are recorded superimposed on the waveform crest. The frequency of pulses appearance, their origin and their magnitude varies. Such pulses can be the result of corona and/or short local discharges and arcs. Although, it is not absolutely safe to conclude whether a pulse is the result of corona discharges or short arcing based only on the leakage current waveform shape, the usual case should be considered to be that smaller pulses are the result of corona discharges while larger pulses are the result of local discharges and arcs.

Several techniques have been applied on leakage current measurements that fall under six general categories: calculation of basic electrical values, advanced time domain analysis techniques, assigning different components, frequency analysis, pattern recognition techniques and the STD_MRA technique. The basic problem is that what is important for the insulation performance is not only the level of leakage current but also the actual

waveform shape. Although in general the level of leakage current increases as activity advances, it is widely accepted that LC magnitude is not a safe indication of electrical activity. Therefore, several leakage current analysis techniques have been proposed, each with its own characteristics, and the behavior of different values has been proposed as an indication for surface activity, condition and overall insulators' performance. Although a fully representative value of the waveform shape is yet to be defined, the vast variety of leakage current monitoring application shows the significance of leakage current as a monitoring and investigating tool.

## REFERENCES


[1] *IEC/TS 60815, Selection and dimensioning of high-voltage insulators intended for use in polluted conditions* (IEC, 2008).

[2] *CIGRE WG 33-04 The measurement of site pollution severity and its application to insulator dimensioning for a.c. systems* // *Electra* **64** (1979) 101.

[3] *CIGRE WG 33-04, TF 01, A review of current knowledge: polluted insulators* (Cigre publications, 1998).

[4] M. Amin, M. Akbar and S. Amin // *Rev. Adv. Mater. Sci.* **16** (2007) 10.

[5] *IEC507, Artificial pollution tests on high-voltage insulators to be used on a.c. systems* (IEC, 1991).

[6] *IEC 60587, Electrical insulating materials used under severe ambient conditions-Test methods for evaluating resistance to tracking and erosion* (IEC, 2007).

[7] *IEC 62217, "Polymeric insulators for indoor and outdoor use with a nominal vlotage > 1000 V – General definitions, test methods and acceptance criteria* (IEC, 2005).

[8] *CIGRE WG B2.03, Guide for the establishment of naturally polluted insulator testing stations* (CIGRE, 2007).

[9] J.L. Fierro-Chavez, I. Ramirez-Vasquez and G. Montoya-Tena // *IEE Proc.-Gener.Transm.Distrib.* **143** (1996) 560.

[10] M. Sato, A. Nakajima, T. Komukai and T. Oyamada, In: *IEEE Conf. Electr. Insul. Dielectr. Phenomena* (CEIDP,1998), p. 64.

[11] M.A.R.M. Fernando and S.M. Gubanski // *IEEE Trans. Dielectr. Electr. Insul.* **6** (1999) 688.

[12] I.J.S. Lopes, S.H. Jayaram and E.A. Cherney // I*EEE Trans. Dielectr. Electr. Insul.* **9** (2002) 964.

[13] M. Otsubo, T. Hashiguchi, C. Honda, O. Takenouchi, T. Sakoda and Y. Hashimoto // *IEEE Trans. Dielectr. Electr. Insul.* **10** (2003) 1053.

[14] Y. Zhu, S. Yamashita, N. Anami and M. Otsubo, In: *Annual Report Conference on Electrical Insulation and Dielectric Phenomena* (2003), p. 62.

[15] A.H. El-Hag, S.H. Jayaram and E.A. Cherney // *IEEE Trans. Dielectr. Electr. Insul.* **10** (2003) 128.

[16] S. Kumagai and N. Yoshimura // *IEEE Trans. Dielectr. Electr. Insul.* **11** (2004) 681.

[17] K Siderakis, D Agoris and S Gubanski // *Journal of Physics D: Applied Physics* **38** (2005) 3682.

[18] I.A. Metwally, A. Al-Maqrashi, S. Al-Sumry and S. Al-Harthy // *Electr. Power Syst. Res.* **76** (2006) 778.

[19] S. Kumagai, B. Marungsri, H. Sinokubo, R. Matsuoka and N. Yoshimura // *IEEE Trans. Dielectr. Electr. Insul.* **13** (2006) 1286.

[20] A.H. El-Hag // *Electr. Power Syst. Res.* **77** (2007) 379.

[21] A.H. El-Hag, A.N. Jahromi and M. Sanaye-Pasand // *Electr. Power Syst. Res.* **78** (2008) 1686.

[22] B.X. Du and Y. Liu // *IEEE Trans. Power. Deliv.* **24** (2009) 1458.

[23] B.X. Du, Y. Liu, H.J. Liu and Y.J. Yang // I*EEE Trans. Dielectr. Electr. Insul.* **16** (2009) 139.

[24] N. Bashir and H. Ahmad // *IEEE Trans. Dielectr. Electr. Insul.* **17** (2010) 819

[25] B. Marungsri, H. Komiya, I. Aoyama, A. Ishikawa and R. Matsuoka, In: *Proceedings of the 7th International Conference on Properties and Applications of Dielectric Materials* (2003), p. 393

[26] M.A.R.M. Fernando and S.M. Gubanski // *IEEE Trans. Dielectr. Electr. Insul.* **17** (20010) 326.

[27] F. Kaidanov and R. Munteanu, In: *Eighteenth Convention of Electrical and Electronics Engineers in Israel*, (1995).

[28] T. Suda // *IEEE Trans. Dielectr. Electr. Insul.* **8** (2001) 705.

[29] B. S. Reddy and G.R. Nagabhushana // *Plasma Sci. Technol.* **5** (2003) 1921.

[30] T. Suda // *IEEE Trans. Power Deliv.* **20** (2005) 481.

[31] S. Chandrasekar, C. Kalaivanan, A. Cavallini and G.C. Montanari // I*EEE Trans. Dielectr. Electr. Insul.* **16** (2009) 574.

[32] J. Li, C. Sun, W. Sima, Q. Yang and J. Hu // *IEEE Trans. Power Deliv.* **25** (2010) 417.
[33] H.H. Kordkheili, H. Abravesh, N. Tabasi, M. Dakhem and M.M. Abravesh // *IEEE Trans. Dielectr. Electr. Insul.* **17** (2010) 502.
[34] J. Li, W. Sima, C. Sun and S.A. Sebo // *IEEE Trans. Dielectr. Electr. Insul.* **17** (2010) 490.
[35] X. Jiang, Y. Shi, C. Sun and Z. Zhang // *IEEE Trans. Dielectr. Electr. Insul.* **17** (2010) 481.
[36] J.H. Kim, W.C. Song, J.H. Lee, Y.K. Park, H.G. Cho, Y.S. Yoo and K.J. Yang // *IEEE Trans. Dielectr. Electr. Insul.* **8** (2001) 1108.
[37] M. Ugur, D.W. Auckland, B.R. Varlow and Z. Emin // *IEEE Trans. Dielectr. Electr. Insul.* **4** (1997) 763.
[38] R. Sarathi, S. Chandrasekar and N. Yoshimura // *IEEE Trans. Power Deliv.* **21** (2006) 243.
[39] L.H. Meyer, S.H. Jayaram and E.A. Cherney // *IEEE Trans. Dielectr. Electr. Insul.* **11** (2004) 424.
[40] S. Gubanski // *IEEE Trans. Electr. Insul.* **25** (1990) 331.
[41] H. Homma, T. Takahashi, T. Taniguchi and K. Izumi, In: *Electrical Electronics Insulation Conference and Electrical Manufacturing & Coil Winding Conference* (1993) p. 655.
[42] H. Homma, T. Kuroyagi, T. Takahashi, S. Obtsuka, M. Ohtsuka and M. Hikita, In: *Annual Report Conference on Electrical Insulation and Dielectric Phenomena* (2002), p. 676.
[43] S. Kumagai, M. Suzuki and N. Yoshimura // *T. IEE Japan* **121-A** (2001) 324.
[44] K. Siderakis and D. Agoris // *Electr. Power Syst. Res.* **78** (2008) 248.
[45] J.P. Holtzhausen and W.L. Vosloo, In: *13th Intern. Sympos. High Voltage Eng. (ISH)* (Milpress, 2003).
[46] W.L. Vosloo, J.P. Holtzhausen and A.H.A. Roediger, In: *IEEE 4th Africon Conf.* **1** (1996) 489.
[47] C.S. Richards, C.L. Benner, K.L. Butler-Purry and B.D. Russell // *IEEE Trans. Power Deliv.* **18** (2003) 551.
[48] E. Fontana, S.C. Oliveira, F.J.M.M. Cavalcanti, R.B. Lima, J.F. Martins-Filho and E. Meneses-Pacheco // *IEEE Trans. Power Deliv.* **21** (2006) 2064.
[49] S.C. Oliveira, E. Fontana and F.J.M.M. Cavalcanti // I*EEE Trans. Power Deliv.* **24** (2009) 2257.
[50] S.C. Oliveira, E. Fontana and F.J.M.M. Cavalcanti // *IEEE Trans. Power Deliv.* **24** (2009) 822.
[51] K.L. Chrzan // *IEEE Trans. Power Deliv.* **25** (2010) 904.
[52] G. Montoya, I. Ramirez and R. Hernandez, In: *Transmission and Distribution Conference and Exhibition* (IEEE/PES, 2008), p.1.
[53] D. Pylarinos, K. Siderakis, E. Pyrgioti, E. Thalassinakis and I. Vitellas // I*EEE Trans. Dielectr. Electr. Insul.* **18** (2011) 122.
[54] D. Pylarinos, K. Siderakis, E. Pyrgioti, E. Thalassinakis and I. Vitellas // *Eng. Technol. Appl. Sci. Res.* **1** (2011) 63.
[55] D. Devendranath, Channakeshava and A.D. Rajkumar // *IEEE Trans. Dielectr. Electr. Insul.* **9** (2002) 294.
[56] F. Meghnefi, C. Volat and M. Farzaneh // *IEEE Trans. Dielectr. Electr. Insul.* **14** (2007) 1381.
[57] Y. Liu and B.X. Du // *IEEE Trans. Dielectr. Electr. Insul.* **17** (2010) 465.
[58] C. Volat, F. Meghnefi, M. Farzaneh and H. Ezzaidi // *IEEE Trans. Dielectr. Electr. Insul.* **17** (2010) 443.
[59] R. Boudissa, S. Djafri, A. Haddad, R. Belaicha and R. Bearch // I*EEE Trans. Dielectr. Electr. Insul.* **12** (2005) 429.
[60] X. Zhang, S.M. Rowland and V. Terzija // *IEEE Trans. Dielectr. Electr. Insul.* **17** (2010) 473.
[61] Y. Zhu, M. Otsubo, C. Honda, Y. Hashimoto and A. Ohno // *IEEE Trans. Dielectr. Electr. Insul.* **12** (2005) 556.
[62] M.A. Douar, A. Mekhaldi and M.C. Bouzidi // *IEEE Trans. Dielectr. Electr. Insul.* **17** (2010) 1284.
[63] K. Siderakis, D. Agoris, E. Pyrgioti and E. Thalassinakis // *WSEAS Trans. on Circuits and Systems* **3** (2004) 1188.
[64] Waluyo, P.M. Pakpahan, Suwarno and M.A. Djauhari // *World Academy of Sci., Eng. Techn.* **32** (2007) 293.
[65] D. Pylarinos, K. Siderakis, E. Pyrgioti, I. Vitellas and E. Thalassinakis, In: *5th International Conference and Technical Exhibit on Deregulated Electricity Market Issues in South-Eastern Europe* (2010).
[66] F. Amarh, G.G. Karady and R. Sundararajan // *IEEE Trans. Power Deliv.* **17** (2002) 1063.
[67] D. Pylarinos, K. Siderakis, E. Pyrgioti, E. Thalassinakis and I. Vitellas // *Eng. Technol. Appl. Sci. Res*. **1** (2011) 8.

[68] M. Amin and M. Salman // *Rev. Adv. Mater. Sci.* **13** (2006) 93.

[69] M. Amin, S. Amin and M. Ali // *Rev. Adv. Mater. Sci.* **21** (2009) 75.